Ultrafast transient dynamics of Zn(II) porphyrins: Observation of vibrational coherence by controlling chirp of femtosecond pulses

Min-Chul Yoon, Dae Hong Jeong, Sung Cho, Dongho Kim, Hanju Rhee, and Taiha Joo

---

Articles you may be interested in

Spectrally- and time-resolved vibrational surface spectroscopy: Ultrafast hydrogen-bonding dynamics at D 2 O / CaF 2 interface
J. Chem. Phys. **122**, 134713 (2005); 10.1063/1.1873652

Spectrally resolved femtosecond two-color three-pulse photon echoes: Study of ground and excited state dynamics in molecules
J. Chem. Phys. **120**, 8434 (2004); 10.1063/1.1651057

Femtosecond pump-probe study of molecular vibronic structures and dynamics of a cyanine dye in solution
J. Chem. Phys. **110**, 12070 (1999); 10.1063/1.479142

Femtosecond dynamics of photoinduced molecular detachment from halogenated alkanes. I. Transition state dynamics and product channel coherence
J. Chem. Phys. **109**, 4415 (1998); 10.1063/1.477045

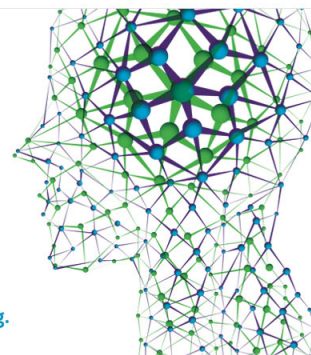Vibrational cooling after ultrafast photoisomerization of azobenzene measured by femtosecond infrared spectroscopy
J. Chem. Phys. **106**, 519 (1997); 10.1063/1.473392

Ultrafast transient dynamics of Zn(II) porphyrins: Observation of vibrational coherence by controlling chirp of femtosecond pulses

Min-Chul Yoon, Dae Hong Jeong, Sung Cho, and Dongho Kim[a)]
National Creative Research Initiatives Center for Ultrafast Optical Characteristics Control and Department of Chemistry, Yonsei University, Seoul 120-749, Korea

Hanju Rhee and Taiha Joo[b)]
Division of Molecular and Life Sciences, Department of Chemistry, Pohang University of Science and Technology (POSTECH), Pohang, 790-784, Korea

Femtosecond coherence spectroscopic study on porphyrin molecules has demonstrated that the oscillatory features residing at the transient absorption and fluorescence decay profiles are strongly correlated with the lifetimes of the excited states and the displacements of the minima of the potential energy surfaces that are involved in the pump and probe laser pulses. We have attained a greater degree of control in the wave packet dynamics in the transient absorption by controlling the chirp of the ultrashort optical pulses. This feature provides a clue to the excited potential energy surface such as its curvature and displacement. For two representative porphyrin monomers, Zn^{II} tetraphenylporphyrin and Zn^{II} octaethylporphyrin, we were able to obtain detailed information on the excited state dynamics and subsequent structural changes based on the comparison between the frequency spectra retrieved from the oscillatory features in the transient absorption and fluorescence temporal profiles and the ground state Raman spectra. © *2003 American Institute of Physics.*
[DOI: 10.1063/1.1524175]

I. INTRODUCTION

Multiporphyrin arrays have been constructed using several types of shorter linkers that are suitable for preparing linear or extended architectures *via meso* position attachment for the possible applications as artificial light harvesting arrays and molecular photonic wires.[1–5] In recent years, a variety of molecular modules have been employed as a construction element of supramolecular rods.[6–8] Among these, porphyrins are one of the most attractive building block elements due to their desirable characteristics such as rigid planar geometry, high stability, intense electronic absorption, and small HOMO-LUMO energy gap.[9,10] Thus it is indispensable to have a deep understanding into the excited states of the porphyrin molecules because light signal transmission in molecular photonic wires proceeds through the excited state energy transfer.[11]

Femtosecond coherence vibrational spectroscopy is based on impulsive excitation of vibrations, which creates a wave packet through coherent superposition of the vibrational states.[12–15] The motion of the wave packet leads to an oscillation of the transition frequency in time. Dephasing and population relaxation result in damping of the wave packet. Various time-resolved spectroscopic techniques such as pump–probe transient absorption (TA) and time-resolved fluorescence by frequency up-conversion can be used to observe the dynamics of a vibrational wave packet motion on potential energy surfaces in real time. In transient absorption measurements, especially when both pump and probe pulses

are in resonance with the same electronic transition, it is generally difficult to assign an oscillation to a vibration in electronically ground or excited state.[16]

Formation of the wave packet is affected by various molecular aspects such as displacement of the vibrational mode between the two electronic states involved (Huang–Rhys factor) and lifetimes of the excited states.[17–19] A vibrational mode with a large Huang–Rhys factor is favored in the wave packet formation. Because the ground state wave packet is created by stimulated Raman process, which consists of two field–matter interactions, the electronic coherence created by the first field–matter interaction needs to propagate (displaced from the original nuclear position) before the second field–matter interaction puts the system to vibrational coherence in the ground state. Accordingly, the wave packet formation in the ground state is attenuated, when the lifetime of the electronically excited state is short compared to the vibrational period. In this case, of course, excited state contribution to the signal is negligible. Pulse duration and temperature can also be varied to manipulate the formation of the wave packets. When the pulse duration is much shorter than the vibrational period, the wave packet formation in the ground state is attenuated due to the same reason as in the case of short excited state lifetime. In this case, excited state wave packets are formed and their dynamics can be observed.

The wave packet formation can also be controlled more actively by pulse shaping techniques. Phase and amplitude masks along with the optimization routine can be employed to control the electric field and to manipulate the wave function robustly. A much simpler yet still useful way to control

[a)]Electronic mail: dongho@yonsei.ac.kr
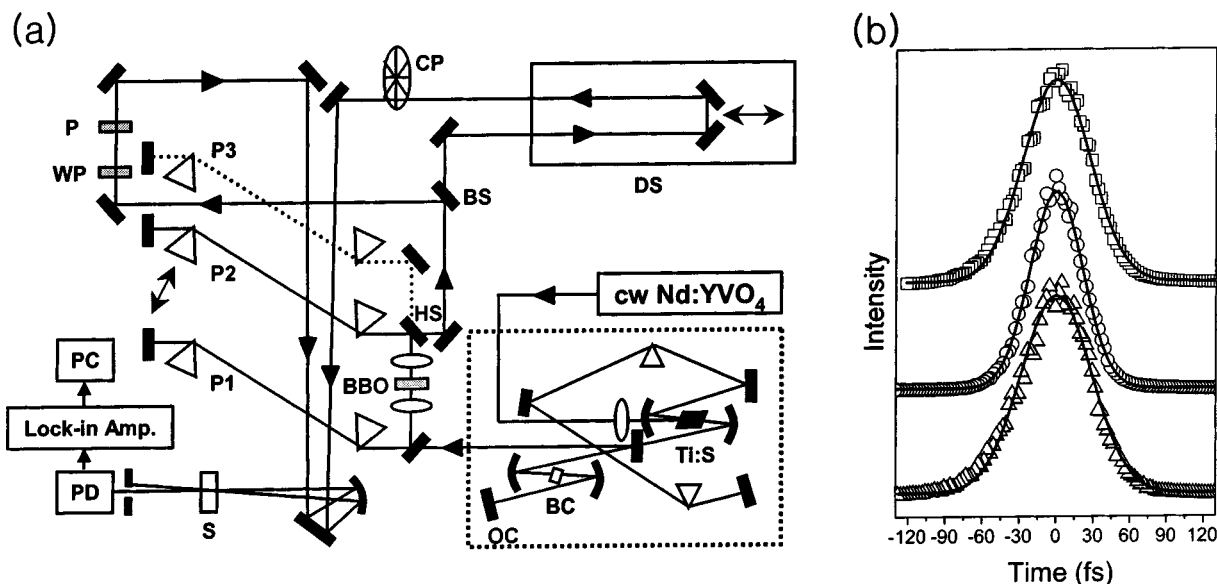[b)]Electronic mail: thjoo@postech.ac.kr

FIG. 1. (a) Experimental setup of femtosecond pump–probe spectroscopy. Homebuilt cavity-dumped mode-locked Ti:sapphire laser is located in the dotted box. Ti:S, Ti:sapphire crystal; BC, Bragg cell; OC, output coupler; BBO, β-BaBO$_3$ nonlinear crystal; HS, harmonic separator; BS, beamsplitter; DS, optical delay stage; CP, chopper; P1–P3, fused silica prism; P, polarizer; WP, half-wave retarder; PD, silicon photodiode. (b) Cross-correlation traces of transform-limited and chirped pulses. Pulse widths of second harmonic pulse are 38.5 (open squares, negatively chirped), 31.4 (open circles, transform-limited), and 38.2 fs (open triangles, positively chirped), respectively.

wave function is to use chirped pulses. In linearly chirped femtosecond pulses, the phase of each frequency component varies linearly in time. By using either positively (blue follows red) or negatively chirped pulses, the arrival time of each frequency component at the sample can be controlled. Wave packet formation with chirped pump pulses has been discussed in detail previously.[20–23] In usual cases, where the excited state potential is displaced to larger nuclear coordinate than the ground state, the optical transition frequency vs nuclear coordinate decreases. A stimulated Raman process is enhanced for negatively chirped (NC) pump pulses, that is, NC pump pulses favor creation of the wave packet in the ground state, whereas positively chirped (PC) pump pulses discriminate against it. On the other hand, the wave packet formation in the excited state is favored by excitation with the shortest possible pulses, transform-limited pulses for a given pulse spectrum. Femtosecond coherence spectroscopy with a control of the chirp of ultrashort pulses is ideally suited for an attempt to reveal the potential energy surfaces of chromophores in which the wave packets are generated and evolved.[20–22]

In transient absorption, the probe wavelength is usually varied to probe either the ground state contribution through ground state bleach components or the excited state contribution through stimulated emission components, though it is not always clear what is being probed.[20–22] Excited state dynamics can be best examined by time-resolved spontaneous emission, although the experimental time resolution of the spontaneous emission measurement is currently limited to ~100 fs, which allows observation of the wave packet motion up to 150 cm^{-1}. Since ground state vibrational frequencies are available from Raman spectra, a comparative study of femtosecond coherent vibrational spectroscopy, time-resolved spontaneous fluorescence, and Raman spectroscopy

of the molecular systems of interest is expected to give detailed understanding on the structural changes occurring in the excited potential energy surfaces.[24,25]

In this paper, we present time-resolved spectroscopic experiments on Zn^{II} porphyrins, including measurements of pump–probe ultrafast transient absorption, fluorescence up-conversion, and Raman spectra. We also report the dependence of oscillatory features on the chirp of ultrashort optical pulses to gain further insight into the potential energy surfaces of various Zn^{II} porphyrins. We have studied impulsively photoinduced vibrational coherent motions on the electronically ground and excited states of two Zn^{II} porphyrins in toluene using chirp-controlled femtosecond pulses; Zn^{II} tetraphenylporphyrin (Zn^{II}TPP), and Zn^{II} octaethylporphyrin (Zn^{II}OEP) which are representative porphyrin monomers (*meso-* versus β-substituted).

II. EXPERIMENT

A. Femtosecond pump–probe setup

Optical layout for the ultrafast transient absorption measurement is displayed in Fig. 1(a). A homemade cavity-dumped Kerr lens mode-locked Ti:sapphire oscillator is shown in the dotted box. An intracavity second-harmonic output at 532 nm of a diode pumped cw Nd:YVO$_4$ laser (5 W, Millennia, Spectra Physics) was focused onto a 10 mm long Ti:sapphire crystal by a 10 cm focal length convex lens. Temperature of the Ti:sapphire crystal was maintained at 15 °C. A prism pair was used to compensate group velocity dispersion (GVD) and to tune the laser wavelength. The mode-locked pulses had a repetition rate of 72 MHz and its averaged output was nearly 200 mW with a 2.5% output coupler. For cavity-dumping, a fused silica Bragg cell controlled by acousto-optic modulation from a rf driver

(CD5000, CAMAC) was used. Typical dumping rate was 200 kHz to avoid thermal and accumulation effects on the sample. Spectral width of the pulses was about 25 nm at the center wavelength of 830 nm and the typical output power was around 20 mW. The cavity-dumped output pulses were compressed by an extra cavity prism pair (P1) to compensate the GVD and focused onto a 100 μm thick BBO crystal. Frequency doubled pulses were recompressed by another pair of prisms (P2) and then split by a broadband pellicle beamsplitter (BS) to serve as pump and probe pulses. The pump pulses were delayed by a motor-controlled translation stage and the polarization of the probe pulses were precisely adjusted by a wave plate and a polarizer. After overlapping at sample position with a very small angle, the probe pulses were detected by a silicon photodiode. Pump-induced transmittance change of the probe pulses was recorded by a lock-in amplifier (DSP7265, EG&G). All measurements were made by using a quartz cell (Hellma) with 1 mm path length.

Residual 830 nm pulses were also recompressed by another fused-silica prism pair. The pulse duration of the second harmonic at 416 nm measured by the cross-correlation with the residual 830 nm pulses using a 200 μm thick BBO crystal was typically 30 fs by assuming a Gaussian envelope function [Fig. 1(b)]. Small residual higher order chirp terms could not be removed perfectly, and we refer to the shortest duration pulse as transform-limited (TL) for the sake of convenience. Chirp of the pump pulses was controlled by adjusting the path length of the prism pair (P2).

B. Time-resolved fluorescence apparatus

For time-resolved fluorescence measurement, the center wavelength of the cavity-dumped pulses was tuned to 812 nm to reduce scattering. The second harmonic (406 nm) of the 812 nm pulse was used as a pump pulse, and the time-resolved fluorescence signal was obtained by frequency up-conversion method using the residual 812 nm pulse as a gate pulse. To observe wave packet dynamics in the electronic excited state, ultrahigh time resolution is required. With ~100 fs time resolution of the fluorescence up-conversion technique reported to date, wave packet dynamics up to 166 cm^{-1} (100 fs to be 1/2 of the vibrational period) can be observed. To achieve higher time resolution, GVD and group velocity mismatch (GVM) must be minimized with a perfect imaging in fluorescence collection. We have improved our fluorescence up-conversion apparatus in several aspects to achieve ~50 fs time resolution. First, GVD in the pump and gate pulses was carefully compensated to achieve short pulse duration at the sample and at the crystal, respectively, for sum frequency generation (SFG). A 100 μm thick BBO crystal was used to minimize GVD. To minimize GVM, which is the dominant mechanism to deteriorate time resolution, non-collinear sum frequency generation scheme is used with the crossing angle of 22° between the gate and fluorescence pulses. We have employed a single reflective microscope objective lens to collect and to focus fluorescence efficiently without aberration. With these improvements, 50 fs time resolution can be achieved.
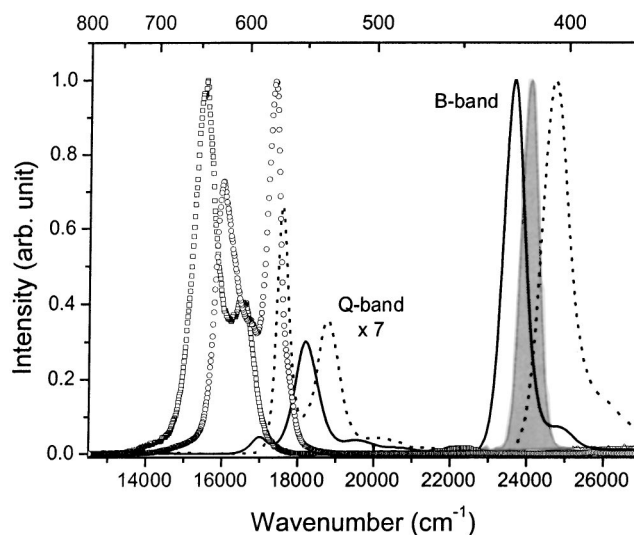

FIG. 2. Steady-state absorption spectra of Zn^{II}TPP (solid line); Zn^{II}OEP (dotted line), and emission spectra of Zn^{II}TPP (open square); Zn^{II}OEP (open circle) in toluene at ambient temperature excited at 400 and 390 nm, respectively. Spectrum of the pump pulse was also included with the FWHM of 11 nm centered at 416 nm (shaded area).

Steady-state absorption and emission spectra were recorded by Shimadzu UV-1601 and Hitach F/4500, respectively, using a 1 cm quartz cell. Raman spectra were recorded by using a He–Cd and Kr$^+$ ion lasers, a 50 cm focal length spectrograph with notch filters and a liquid nitrogen cooled CCD detector.

Zn^{II}TPP and Zn^{II}OEP were purchased from Porphyrin Product (Logan, UT) and used as received. All measurements were performed at ambient temperature (22 ± 1 °C).

III. RESULTS

A. Electronic structure

Metalloporphyrins exhibit well-resolved two singlet absorption bands in visible region. An intense B (S_2, Soret) band is located around 400 nm, and usually much weaker Q (S_1) band appears around 500–600 nm. All these transitions are assigned to porphyrin (π–π^*) transitions. Figure 2 shows the steady-state absorption and emission spectra of Zn^{II}TPP and Zn^{II}OEP in toluene. Absorption center frequencies of both B- and Q-bands of Zn^{II}TPP appear at lower energies than those of Zn^{II}OEP. It is noteworthy that the spectral width of the B-band of Zn^{II}TPP is slightly narrower than that of Zn^{II}OEP. In contrast to the single B-band, Q-bands show vibrational progressions. Zn^{II}TPP has a relatively strong $Q(1,0)$ band and weak $Q(0,0)$ and $Q(2,0)$ bands. On the other hand, the $Q(0,0)$ band of Zn^{II}OEP is much stronger than the other vibronic bands. The steady-state emission spectra are dominated by the Q-band fluorescence. The absorption and emission spectra are in mirror image indicating similar structures between the ground and Q-states. Emission from the Q-band is strong with the fluorescence quantum yields (Φ_{S_1}) of 0.03 and 0.04 for Zn^{II}TPP and Zn^{II}OEP, respectively.[26] Zn^{II}TPP shows relatively strong B-band emission at 430 nm, whereas no B-band emission is observed for Zn^{II}OEP. From the absorption and emission

TABLE I. Photophysical data from electronic absorption and emission spectra of $Zn^{II}TPP$ and $Zn^{II}OEP$ in toluene.

	$Zn^{II}TPP$		$Zn^{II}OEP$	
	S_2	S_1	S_2	S_1
Absorption maximum (nm)	423	549; $Q(1,0)$ 587; $Q(0,0)$	405	533; $Q(1,0)$ 569; $Q(0,0)$
Emission maximum (nm)	432	605; $Q(0,0)$ 645; $Q(0,1)$	...	576; $Q(0,0)$ 625; $Q(0,1)$
$\Delta(S_n - S_0)$ (cm^{-1})	493	507[a](2711)	...	213
τ_{Sn}	1.2 ps[b]	2.54 ns[c,d]	<20 fs[e]	2.3 ns[d]
Φ_{Sn}	1.5×10^{-3}	0.03[c,d]	$<10^{-6}$ [e]	0.04[d]

[a]Calculated from the 0–0 band absorption and emission. 2711 cm^{-1} by the most intense 0–1 band.

[b]Fluorescence up-conversion data.

[c]Reference 27.

[d]Reference 28 (in chloronaphthalene).

[e]Estimated value from Raman data.

spectra, the Stokes shifts were estimated. Although the emission properties of the B-states of $Zn^{II}TPP$ and $Zn^{II}OEP$ are somewhat different, the fluorescence lifetimes and quantum yields of the Q-states of $Zn^{II}TPP$ and $Zn^{II}OEP$ are similar. All the photophysical parameters are summarized in Table I.

B. Femtosecond coherence spectroscopy

Femtosecond pump–probe spectroscopy gives a direct insight into the coherent dynamics of vibrational wave packet motions and subsequent vibronic relaxation processes in condensed phase. We have studied impulsively excited coherent vibrational motions on the electronically ground and excited states of $Zn^{II}TPP$ and $Zn^{II}OEP$ in toluene using chirp-controlled femtosecond pulses.

Figure 3(a) shows one-color transient absorption signal of the B-band of $Zn^{II}TPP$ at 416 nm. Coherent spikes are dominant around the zero-delay time, and prominent high-frequency oscillations are superposed on the temporal profiles damping within 1 ps. It is also apparent that the amplitude of the oscillations is significantly affected by the chirp of the pump pulses. The cross-correlation traces show the

shortest pulse duration of ~30 fs (chirp free), which broadens to ~40 fs with the GVD of ±250 fs (Ref. 2) for either the PC or NC pulses, respectively. Compared to the TL pulses, a significant enhancement of the oscillation amplitudes was observed in the case of the NC pump pulse excitation, although the pulse duration was longer than the TL pulses. Since the wave packet in the S_2 state is moving from higher to lower transition frequencies, this process is enhanced when red follows blue. For the PC pump pulses, the oscillation amplitudes were diminished compared to the case of the TL pulse excitation.

Figure 3(b) shows the temporal profiles of the transient absorption of $Zn^{II}OEP$ at 406 nm. Coherent spikes are also observed around the zero-delay time, and relatively weak oscillations compared to $Zn^{II}TPP$ are observed in the transient absorption signals. Moreover, the oscillatory feature was not enhanced as the chirp of the pump pulses was varied: TL pump pulses give rise to slightly stronger oscillations than PC or NC pump pulses. A successful measurement of the Raman spectrum of $Zn^{II}OEP$ by 406.7 nm excitation without fluorescence interference indicates that the S_2 state is very short lived and its lifetime is estimated to be shorter than ~20 fs. Since the excited state lifetime is shorter than the pulse duration, the entire transient absorption signal of $Zn^{II}OEP$ arises from the ground state bleach contribution except around time zero, and the oscillation is due to the wave packet motions in the ground state. Therefore, the shortest pulse excitation is advantageous in preparing the wave packets in the ground state of $Zn^{II}OEP$ over the NC or PC pump pulses.

Nuclear and electronic dynamics of the electronically excited state can be best investigated by time-resolved spontaneous fluorescence. Figure 4 shows the time-resolved S_2 state spontaneous fluorescence of $Zn^{II}TPP$ in toluene. Pump pulses were centered at 406 nm near the blue edge of the B-band and the fluorescence was detected at 430 nm. The signal shows initial rise and subsequent decay. The signal can be fitted precisely by exponential rise and decay components with the time constants of 89 fs and 1.2 ps, respectively. The rise component may be assigned to the spectral relaxation caused by solvation and vibrational relaxation pro-
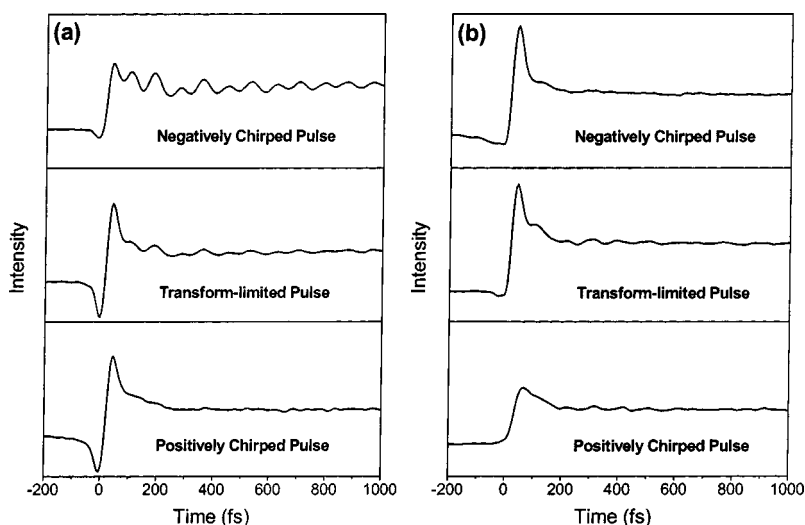

FIG. 3. The temporal profiles of the transient absorption signals by the one-color pump–probe experiment for (a) $Zn^{II}TPP$ at 416 nm and (b) $Zn^{II}OEP$ at 406 nm in toluene by controlling the chirp of the ultrashort optical pulses. [Negatively chirped (top), Fourier transform-limited (middle), and positively chirped optical pulses (bottom).]
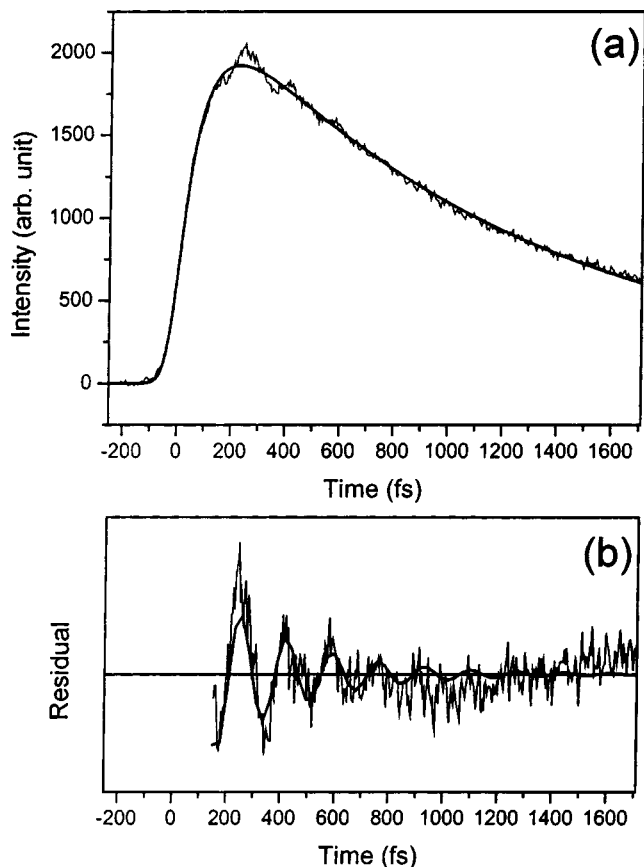
FIG. 4. (a) Time-resolved fluorescence up-conversion profile of $Zn^{II}TPP$ in toluene. Instrumental time-resolution was measured to be about 60 fs. Smooth solid line represents a best-fitted population component having a rise time of 89 fs and a decay time of 1.2 ps. (b) Oscillatory component by subtracting the fitted population component from raw data. A damped sinusoidal fitting curve shows oscillation frequencies of 202 and 383 cm^{-1} with the damping time constants of 220 and 640 fs, respectively.
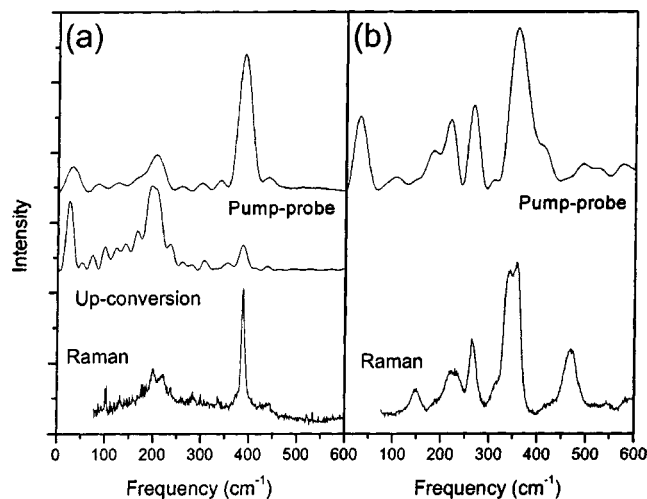

FIG. 5. Fourier-transformed power spectra from the oscillatory features in the temporal profiles of the pump–probe transient absorption signals (top), and resonance Raman spectra (bottom) of (a) $Zn^{II}TPP$ and (b) $Zn^{II}OEP$ in toluene with photoexcitation at 441.6 and 406.7 nm, respectively. Power spectrum of fluorescence up-conversion of $Zn^{II}TPP$ is placed at the middle of (a).

cesses, while the 1.2 ps decay is due to the $S_2 \rightarrow S_1$ internal conversion.[29–31]

Since coherence spikes contribute to the signal around the zero-delay time in the transient absorption decay profiles, they were excluded in the fitting process. To obtain the oscillation spectra of the transient absorption and fluorescence decay profiles, an exponential contribution was subtracted using the following equation:

$$\Delta A(t) = A \exp(-t/\tau) + B. \qquad (1)$$

Then, the residuals were Fourier transformed to yield the frequency spectra shown in Fig. 5. Oscillation frequencies retrieved from the spectra with the help of linear prediction singular value decomposition (LPSVD) analyses[32] are listed in Table II. For $Zn^{II}TPP$, the spectra are dominated by two totally-symmetric vibrational modes at 207 and 389 cm^{-1} with the damping time constants of 340 and 600 fs, respectively. $Zn^{II}OEP$ shows more complicated spectrum compared to $Zn^{II}TPP$. In the case of fluorescence decay of $Zn^{II}TPP$, Fourier transform [Fig. 4(b)] and LPSVD analyses [Fig. 5(a)] yield two oscillation frequencies, 202 and 383 cm^{-1}, with the damping time constants of 220 and 640 fs, respectively.

C. Resonance Raman spectra

Resonance Raman (RR) spectrum of $Zn^{II}TPP$ shown in Fig. 5(a) was obtained with photoexcitation at 441.6 nm from a He–Cd laser, which corresponds to the low-energy tail of the B-band. The ground state Raman spectra with photoexcitation at 406.7 and 413.1 nm from a Kr^+ ion laser were severely obscured by the strong S_2 fluorescence of $Zn^{II}TPP$. The RR spectrum identifies one prominent peak at 388 cm^{-1} along with two weak bands at 201 and 221 cm^{-1}. The Raman frequencies roughly match with the oscillation frequencies observed in the transient absorption and time-resolved fluorescence, where two lower frequency Raman bands appear as a broad single band. The Raman bands at 388 and 201 cm^{-1} are assigned to the metal-pyrrole breathing mode (ν_8) and the phenyl translation mode (ϕ_{10}) on the basis of assignments of $Ni^{II}TPP$.[33,34] These two Raman modes are totally symmetric A_{1g} modes, and thus resonance-activated via the Albrecht A-term scattering.[35] However, no other vibrational modes with A_{1g} symmetry are found in this spectral region. Generally out-of-plane modes are observed in the low frequency region via resonance activation with an aid of symmetry lowering followed by porphyrin distortion.[33,34,36] Slight distortion of porphyrin plane can cause symmetry lowering from ideal D_{4h} to D_{2d}, S_4 or C_{4v} symmetry. Since the solvent is noncoordinating solvent (toluene), it is not relevant to consider doming distortion (C_{4v}) by solvent coordination. $Zn^{II}TPP$ can be slightly distorted from ideally planar structure to saddled or ruffled structures just like $Ni^{II}TPP$,[35,36] leading to symmetry lowering from D_{4h} to D_{2d} (saddled) and to S_4 (ruffled). In saddled structure (D_{2d}) B_{1u} modes become A_1 modes, and in ruffled structure (S_4) B_{1u} and B_{2u} modes become A_1 modes. The most probable candidate for the 221 cm^{-1} band is the pyrrole-tilting mode, γ_{16} (B_{2u}) that was assigned to the 251 cm^{-1} band in

TABLE II. Vibrational frequencies obtained by LPSVD and Fourier-transform analyses of pump–probe and fluorescence up-conversion data and ground state Raman measurement.

	Zn^{II}TPP			Zn^{II}OEP		
Mode	Pump–probe	Up-conversion	Raman[a]	Mode	Pump–probe	Raman[b]
$\phi_{10}(A_{1g})$	207 (340 fs)[c]	202 (220 fs)[c]	201	$\nu_{35}(B_{2g})$	152	147
$\gamma_{16}(B_{2u})$	⋯	⋯	221	$\gamma_{24}(oop)$	218 (680 fs)[c]	226
$\gamma_{12}(B_{1u})$	⋯	⋯	336	$\nu_9(A_{1g})$	259 (1400 fs)[c]	266
$\nu_8(A_{1g})$	389 (600 fs)[c]	383 (640 fs)[c]	388	$\nu_8(A_{1g})$	⋯	338
				$\nu_8(A_{1g})$	354 (300 fs)[c]	357
				$\delta_4(B_{2u})$	⋯	468

[a]Raman data with photoexcitation at 441.6 nm of a cw He–Cd laser.
[b]Raman data with photoexcitation at 406.7 nm of a cw Kr$^+$ laser.
[c]Dephasing time constant of oscillation.

Ni^{II}TPP.[35] We can also observe a weakly activated out-of-plane band at 336 cm^{-1}, which is assigned to the pyrrole-swiveling mode, γ_{12} (B_{1u}).[35]

RR spectrum of Zn^{II}OEP by 406.7 nm excitation is also shown in Fig. 5(b). Similar to Zn^{II}TPP, strong ν_8 band corresponding to the pyrrole-ring breathing mode appears but splits into 338 and 357 cm^{-1} as in Ni^{II}OEP mainly due to the ethyl conformational isomers (triclinic A and B, respectively).[37] The doublet feature is, even though not so prominent as the ν_8 mode, also observed in the asymmetric band shape of the ν_9 mode at 266 cm^{-1}. The ν_8 and ν_9 modes are strongly coupled to metal-pyrrole breathing and C_β-ethyl bending motions. Thus, they are sensitive to the conformational heterogeneity and pyrrole movement. In contrast to Zn^{II}TPP, however, several nontotally symmetric modes are observed in the low frequency region. The RR bands at 147, 226, and 468 cm^{-1} are the pyrrole-translation modes with B_{2g} symmetry (ν_{35}), the $C_\alpha - C_m$ wagging vibration with E_g symmetry (γ_{24}), and the $C_\beta - C_1 - C_2$ bending motion with B_{2u} symmetry (δ_4), respectively.[37] When the symmetry is lowered to C_{2h} (triclinic A or B), B_{1g} symmetry becomes A_g, and E_g symmetry is correlated with $A_g + B_g$. Therefore, B_{1g} and E_g modes are resonance-enhanced via the Albrecht A-term.[35]

IV. DISCUSSION

TA studies employing chirped femtosecond pulses have been applied to gas and solution phase iodine and several dyes in solution as an effort to control the wave packets.[20,21,38–41] Bardeen and co-workers[20,21] have reported chirp controlled transient absorption studies of nile blue and rhodopsin. In the present work, the chirp of pump pulses was adjusted to control the wave packets, and the wave packets created in the ground and excited states are compared to the ground state Raman spectra and the time-resolved spontaneous fluorescence to interrogate the wave packets created separately in each state.

In addition to the active control of the wave packets by chirping of the optical pulses, the creation of the wave pack-

ets was controlled passively by the molecular characteristics, i.e., ultrashort lifetime of the excited state. To illustrate the effect of the excited state lifetime on the wave packets in the ground state clearly, the TA signals including finite pulse duration were calculated. Detailed descriptions on the calculation of the third order nonlinear signals using a nonlinear response function theory have been reported by several authors.[19,42] We have calculated the TA signal for a model transition frequency function $M(t)$ which consists of a critically damped Brownian oscillator and an exponential component to account for intermolecular solvation processes and oscillations for intramolecular vibration,

$$M(t) = \Delta_{BO}^2(1 + \gamma t/2) \cdot \exp(-\gamma t/2) + \Delta_e^2 \exp(-t/\tau_e)$$
$$+ \Delta_v^2 \exp(-t/\tau_v)\cos(\omega t).$$

Figure 6 shows the calculated TA signal for 30 fs TL pulses when the lifetime of the excited state is 10 fs. The damping constant γ for the Brownian oscillator is 80 cm^{-1}, $\tau_e = 3$ ps, $\tau_v = 2$ ps, and $\omega = 300$ cm^{-1}. Coupling strengths are set to be $\Delta_{BO} = 190$ cm^{-1}, $\Delta_e = 190$ cm^{-1}, and $\Delta_v = 120$ cm^{-1}, which reproduces the B-band absorption appropriately.
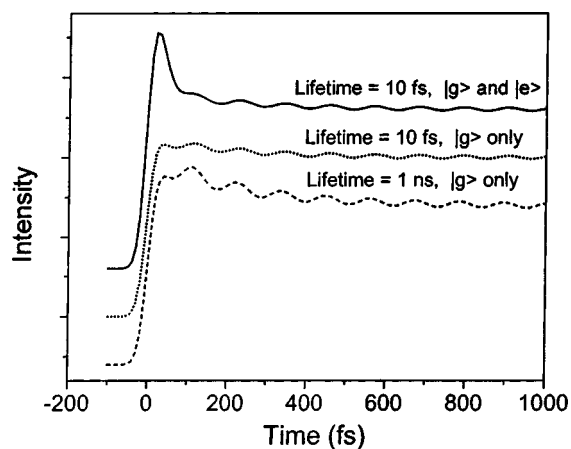

FIG. 6. Calculated transient absorption signals of Zn^{II}OEP with varying the excited state lifetime and the contribution of each electronic state.

A TA signal with longer lifetime was calculated as a reference. The total TA signal reproduces the measured TA signal of $Zn^{II}OEP$ appropriately, showing clearly that the initial spike is due to the short lifetime of the excited state. More importantly, the amplitudes of the oscillatory components in the ground state bleach recovery decreases by 50% as the lifetime is reduced to 10 fs compared to the situation where the lifetime is long.

The oscillation amplitudes of the TA signal in $Zn^{II}OEP$ with TL pulses were diminished by ~50% compared to those in $Zn^{II}TPP$. The lifetime of the *B*-state in $Zn^{II}OEP$ could be estimated by assuming that the vibrational contributions of $Zn^{II}TPP$ and $Zn^{II}OEP$ excluding lifetime effect are about the same. Since the calculated signal with the lifetime of 10 fs gives roughly 50% attenuation of the oscillation, the lifetime of $Zn^{II}OEP$ was estimated to be 10 fs. That is, the lifetime is much shorter than the period of the highest frequency vibration accessible in this experiment. Therefore, the shortest pulse excitation is advantageous in preparing the wave packets in the ground state of $Zn^{II}OEP$ over the NC or PC pump pulses, which is consistent with our observation [Fig. 3(b)].

In order to investigate the structural changes in the excited S_2 state of $Zn^{II}TPP$, we have compared the fast Fourier transform (FFT) power spectra with the ground state Raman spectrum [Fig. 5(a)]. The observed FFT spectra of $Zn^{II}TPP$ are largely in a good accordance with the ground state Raman spectrum. A careful examination of the frequency changes, however, reveals that the vibrational frequency of the ν_8 mode retrieved from the fluorescence decay is slightly lower by ~5 cm^{-1} than that by the TA measurement and ground state Raman spectrum. The ν_8 mode originates from the totally symmetric metal-pyrrole breathing mode that is sensitive to the metal–N distance[43,44] like the other structure sensitive bands (ν_2, ν_{10}, ν_3, and ν_4) especially in electronically excited states.[24,25] The frequency shift of the ν_8 mode is believed to be due to the antibonding character involving the $e_g(\pi^*)$ orbital of the S_2 state of $Zn^{II}TPP$. Thus, this demonstrates the feasibility of femtosecond coherence spectroscopy to probe the structural changes occurring in excited states. On the other hand, since two modes (ϕ_{10} and γ_{16}) appear lying closely in the ground state Raman spectrum, the origin for the bands at 207 and 202 cm^{-1} retrieved from the TA and fluorescence decay, respectively, cannot be exclusively assigned to one mode (Table II). Thus it is difficult to assert the structural changes from these two bands. Meanwhile, a lack of the S_2 emission in $Zn^{II}OEP$ indicates that the excited S_2 state of $Zn^{II}OEP$ is very short-lived (<20 fs) and thus the FFT spectrum obtained by the TA measurement is solely contributed by the ground state. The discrepancies in frequencies between the FFT and ground state Raman spectra of $Zn^{II}OEP$ are presumably due to weaker oscillatory features residing on the TA decay profile of $Zn^{II}OEP$ and $Zn^{II}TPP$.

The observation that, for a given pulse width, positively or negatively chirped pulses yield very different signals indicates that these effects are not just due to the temporal broadening of the pulses. In fact, the intensity of the vibrational coherence is likely to be strongly correlated with the relative positions of the S_0 and S_2 state potentials. In order to
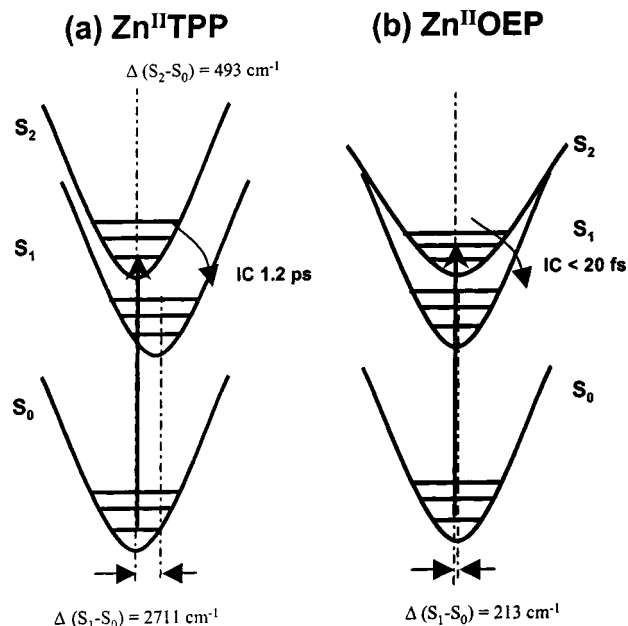

FIG. 7. Schematic illustration of potential energy surfaces of (a) $Zn^{II}TPP$ and (b) $Zn^{II}OEP$.

gain further insight into the potential energy surfaces of the S_2 state it is necessary to collectively consider the optical parameters including Stokes shifts, spectral broadenings, and internal conversion rates. The S_2 emission of $Zn^{II}TPP$ shows 493 cm^{-1} Stokes shift from the corresponding absorption while the S_1 emission of $Zn^{II}TPP$ shows the 2711 cm^{-1} Stokes shift. This reflects that the S_2 excited state potential is much less displaced from the ground state than the S_1 excited state. Prominent observation of the S_2 emission reveals that the internal conversion from the S_2 to S_1 state of $Zn^{II}TPP$ is not efficient relative to that of $Zn^{II}OEP$. Considering these features the schematic potential energy surfaces of $Zn^{II}TPP$ are depicted in Fig. 7(a). The fact that the *B*-band is narrower than the *Q*-band of $Zn^{II}TPP$ seems to be consistent with the inefficient nonradiative decay from the S_2 to S_1 state of $Zn^{II}TPP$. In the case of $Zn^{II}OEP$ the S_1 emission exhibits 213 cm^{-1} Stokes shift, which is smaller than that of $Zn^{II}TPP$. This indicates that the S_1 potential energy surface of $Zn^{II}OEP$ is less displaced from the ground potential energy surface than that of $Zn^{II}TPP$. The broader feature of the *B*-band than the *Q*-band reflects that the curvature of the S_2 potential energy surface is milder than the S_1 potential energy surface. A lack of the S_2 emission of $Zn^{II}OEP$ indicates that the nonradiative decay from the S_2 to S_1 state is very fast, which reflects a strong coupling between the S_2 and S_1 states of $Zn^{II}OEP$. The schematic potential energy surfaces of $Zn^{II}OEP$ illustrating these phenomena are also depicted in Fig. 7(b) even though the position of the S_2 potential energy surface relative to the ground state cannot be unequivocally defined. Although no direct measurement of the displacement between the S_2-S_0 potential energy minima from the S_2 emission is possible with out current experimental technique, we can anticipate that the displacement of the potential energy surface should be very small based on a negligible displacement between the S_1 and S_0 states of $Zn^{II}OEP$

J. Chem. Phys., Vol. 118, No. 1, 1 January 2003

Dynamics of Zn(II) porphyrins   171

(213 cm^{-1}). From the estimated S_2 fluorescence quantum yield and a successful Raman measurement with photoexcitation at the B-band without any interference from the S_2 emission, the upper bound for the S_2 lifetime for Zn^{II}OEP is likely to be <20 fs. Thus, the ultrafast relaxation (<20 fs) of the S_2 state of Zn^{II}OEP arises from a strong coupling between the S_2 and S_1 states aided by the vibrational motions of the ethyl groups substituted at eight β-positions of the porphyrin macrocycle.

V. CONCLUSION

Our present study demonstrates that the signal intensity of the oscillatory feature in the transient absorption decay is strongly associated with the displacements of the minima of the potential energy surfaces that are involved in the pump and probe laser pulses. By using tailored optical pulses in frequency domain, we were able to manipulate the wave packet dynamics which are strongly related to the curvature and displacement of the excited potential energy surfaces. In two representative porphyrins, Zn^{II}TPP and Zn^{II}OEP, we observed that the S_2 state dynamics are much different from each other. Not only the origin of the vibrational coherence but its relationship with the Raman spectrum is expected to give a better understanding on the excited dynamics and structural change of porphyrins.

ACKNOWLEDGMENTS

[1] V. S.-Y. Lin, S. G. DiMagno, and M. J. Therien, Science **264**, 1105 (1994).

[2] A. Osuka, S. Marumo, N. Mataga, S. Taniguchi, T. Okada, I. Yamazaki, Y. Nishimura, T. Ohno, and K. Nozaki, J. Am. Chem. Soc. **110**, 4454 (1998).

[3] N. Aratani, A. Osuka, Y. H. Kim, D. H. Jeong, and D. Kim, Angew. Chem. Int. Ed. Engl. **39**, 1458 (2000).

[4] Y. H. Kim, D. H. Jeong, D. Kim, S. C. Jeoung, H. S. Cho, S. K. Kim, N. Aratani, and A. Osuka, J. Am. Chem. Soc. **123**, 76 (2001).

[5] H. S. Cho, N. W. Song, Y. H. Kim, S. C. Jeoung, S. Hahn, D. Kim, S. K. Kim, N. Yoshida, and A. Osuka, J. Phys. Chem. A **104**, 3287 (2000).

[6] R. W. Wagner, J. S. Lindsey, J. Seth, V. Palaniappan, and D. F. Bocian, J. Am. Chem. Soc. **118**, 3996 (1996).

[7] R. W. Wagner and J. S. Lindsey, J. Am. Chem. Soc. **116**, 9759 (1994).

[8] R. E. Martin and F. Diederich, Angew. Chem. Int. Ed. Engl. **38**, 1350 (1999).

[9] M. R. Wasielewski, Chem. Rev. **92**, 435 (1992).

[10] M. G. H. Vicente, L. Jaquinod, and K. M. Smith, Chem. Commun. **1999**, 1771.

[11] H. S. Cho, D. H. Jeong, M.-C. Yoon, Y. H. Kim, Y.-R. Kim, D. Kim, S. C. Jeoung, S. K. Kim, N. Aratani, H. Shinmori, and A. Osuka, J. Phys. Chem. A **105**, 4200 (2001).

[12] F. Rosca, A. T. N. Kumar, D. Ionascu, X. Ye, A. A. Demidov, and P. M. Champion, Bull. Chem. Soc. Jpn. **75**, 1093 (2002).

[13] X. Ye, A. Demidov, and P. M. Champion, J. Am. Chem. Soc. **124**, 5914 (2002).

[14] F. Rosca, A. T. N. Kumar, X. Ye, T. Sjodin, A. A. Demidov, and P. M. Champion, J. Phys. Chem. A **104**, 4280 (2000).

[15] A. T. N. Kumar, L. Zhu, J. F. Christian, A. A. Demidov, and P. M. Champion, J. Phys. Chem. A **105**, 7847 (2001).

[16] C.-K. Min, T. Joo, M.-C. Yoon, C. M. Kim, Y. N. Hwang, D. Kim, N. Aratani, N. Yoshida, and A. Osuka, J. Chem. Phys. **114**, 6750 (2001).

[17] W. T. Pollard and R. A. Mathies, Annu. Rev. Phys. Chem. **43**, 497 (1992).

[18] D. M. Jonas, S. E. Bradforth, S. A. Passino, and G. R. Fleming, J. Phys. Chem. **99**, 2594 (1995).

[19] S. Mukamel, in *Principles of Nonlinear Optical Spectroscopy* (Oxford, New York, 1995).

[20] C. J. Bardeen, Q. Wang, and C. V. Shank, Phys. Rev. Lett. **75**, 3410 (1995).

[21] C. J. Bardeen, Q. Wang, and C. V. Shank, J. Phys. Chem. A **102**, 2759 (1998).

[22] W. T. Pollard, S. Y. Lee, and R. A. Mathies, J. Chem. Phys. **92**, 4012 (1990).

[23] U. Banin, A. Barona, S. Ruhman, and R. Kosloff, J. Chem. Phys. **101**, 8461 (1994).

[24] S. Sato and T. Kitagawa, Appl. Phys. B: Lasers Opt. **59**, 415 (1994).

[25] V. A. Walters, J. C. de Paula, G. T. Bobcock, and G. E. Leroi, J. Am. Chem. Soc. **111**, 8300 (1989).

[26] G. Szintay and A. Horvth, Inorg. Chim. Acta **310**, 175 (2000).

[27] A. Harriman, G. Porter, and N. Searle, J. Chem. Soc., Faraday Trans. **275**, 1515 (1979).

[28] J. R. Darwent, P. Douglas, A. Harriman, G. Porter, and M. C. Richoux, Coord. Chem. Rev. **44**, 83 (1982).

[29] G. G. Gurzadyan, T.-H. Tran-Thi, and T. Gustavsson, J. Chem. Phys. **108**, 385 (1998).

[30] N. W. Song, H. S. Cho, M.-C. Yoon, S. C. Jeoung, N. Yoshida, A. Osuka, and D. Kim, Bull. Chem. Soc. Jpn. **75**, 1023 (2002).

[31] H.-Z. Yu, J. S. Baskin, and A. H. Zewail, J. Phys. Chem. A **106**, 9845 (2002).

[32] H. Barkhuijsen, R. de Beer, W. M. M. J. Bovée, and D. van Ormondt, J. Magn. Reson. **61**, 465 (1985).

[33] T. S. RushIII, P. M. Kozlowski, C. A. Piffat, R. Kumble, M. Z. Zgierski, and T. G. Spiro, J. Phys. Chem. B **104**, 5020 (2000).

[34] X.-Y. Li, R. S. Czernuszewicz, J. R. Kincaid, and T. G. Spiro, J. Am. Chem. Soc. **111**, 7012 (1989).

[35] A. C. Albercht, J. Chem. Phys. **34**, 1476 (1961).

[36] S. Choi and T. G. Spiro, J. Am. Chem. Soc. **105**, 3683 (1983).

[37] X.-Y. Li, R. S. Czernuszewicz, J. R. Kincaid, P. Stein, and T. G. Spiro, J. Phys. Chem. **94**, 47 (1990).

[38] P. Farmanara, H.-H. Ritze, V. Stert, and W. Radloff, Chem. Phys. Lett. **307**, 1 (1999).

[39] K. Misawa and T. Kobayashi, J. Phys. Chem. **113**, 7546 (2000).

[40] V. V. Lozovoy, B. I. Grimberg, E. J. Brown, I. Pastirk, and M. Dantus, J. Raman Spectrosc. **31**, 41 (2000).

[41] C. J. Bardeen, V. V. Yakovlev, J. A. Squier, and K. R. Wilson, J. Am. Chem. Soc. **120**, 13023 (1998).

[42] T. Joo, Y. Jia, J.-Y. Yu, M. J. Lang, and G. R. Fleming, J. Chem. Phys. **104**, 6089 (1996).

[43] E. Unger, M. Beck, R. J. Lipski, W. Dreybrodt, C. J. Medforth, K. M. Smith, and R. Schweitzer-Stenner, J. Phys. Chem. B **103**, 10022 (1999).

[44] W. Jentzen, M. C. Simpson, J. D. Hobbs *et al.*, J. Am. Chem. Soc. **117**, 11085 (1995).